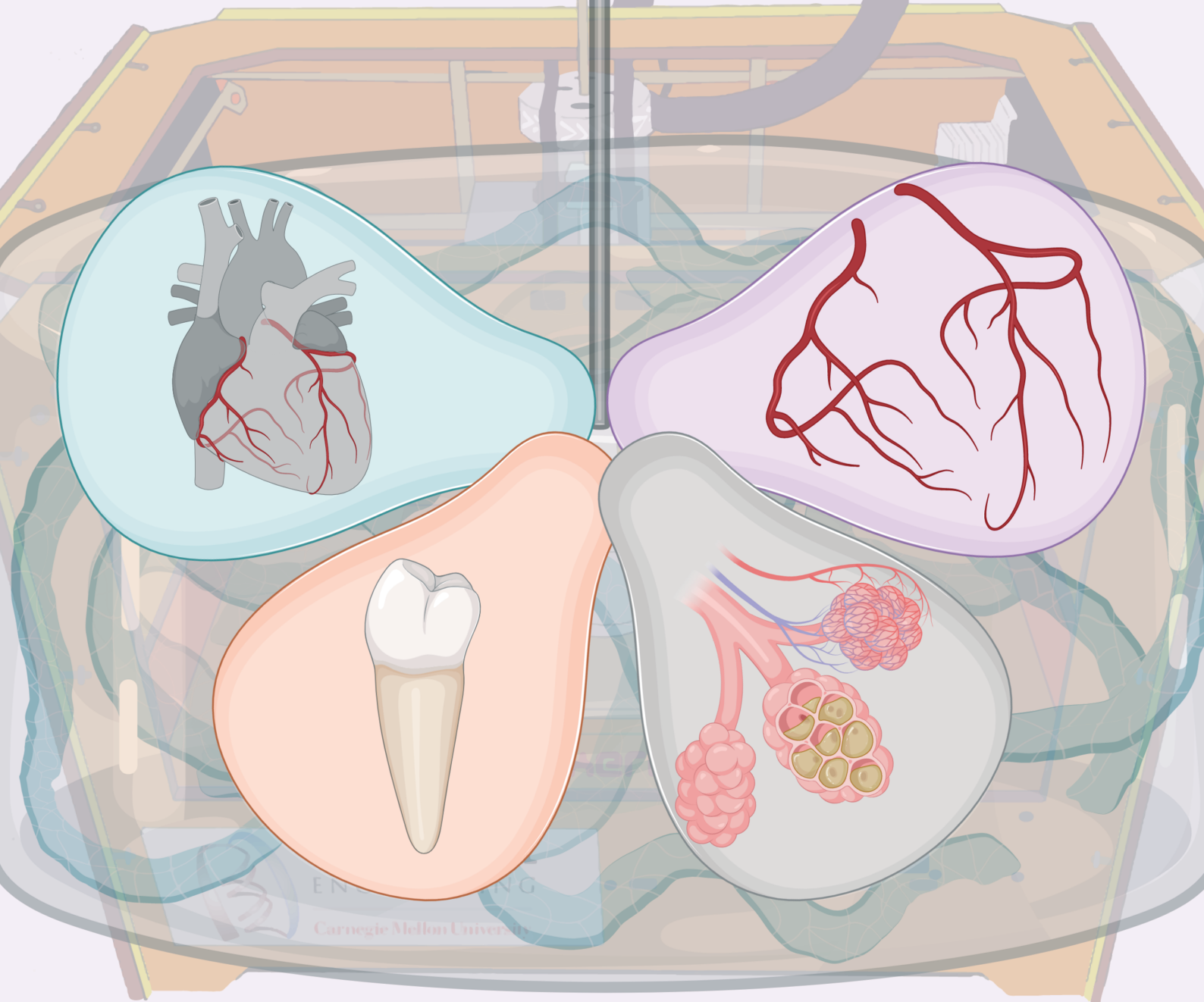


# ADVANCED HEALTHCARE MATERIALS



# 3D Printing Silicone Elastomer for Patient-Specific Wearable Pulse Oximeter

Sara Abdollahi, Eric J. Markvicka, Carmel Majidi, and Adam W. Feinberg\*

Commercial pulse oximeters are used clinically to measure heart rate and blood oxygen saturation and traditionally made from rigid materials. However, these devices are unsuitable for continuous monitoring due to poor fit and mechanical mismatch. Soft materials that match the elastic properties of biological tissue provide improved comfort and signal-to-noise but typically require molding to manufacture, limiting the speed and ease of customizing for patient-specific anatomy. Here, freeform reversible embedding (FRE) 3D printing is used to create polydimethylsiloxane (PDMS) elastomer cuffs for use on the hand and foot. FRE enables printing liquid PDMS prepolymer in 3D geometries within a sacrificial hydrogel bath that provides support during cure. This serves as proof-of-concept for fabricating patient-specific pulse oximeters with pressure sensing, termed P<sup>3</sup>-wearable. A sizing analysis establishes dimensional accuracy of FRE-printed PDMS compared to anatomical computer-aided design models. The P<sup>3</sup>-wearable successfully outputs photoplethysmography (PPG) and pressure amplitude signals wirelessly to a tablet in real time and the PPG is used to calculate heart rate, blood oxygen content, and activity state. The results establish that FRE printing of PDMS can be used to fabricate patient-specific wearable devices and measure heart rate and blood oxygenation on par with commercial devices.

## 1. Introduction

Traditional pulse oximeters are used in the clinic to measure vital signs such as heart rate and peripheral capillary oxygen

Dr. S. Abdollahi, Prof. A. W. Feinberg  
Department of Biomedical Engineering  
Carnegie Mellon University  
5000 Forbes Avenue, Pittsburgh, PA 15213, USA  
E-mail: feinberg@andrew.cmu.edu

Dr. E. J. Markvicka, Prof. C. Majidi  
Robotics Institute  
Carnegie Mellon University  
5000 Forbes Avenue, Pittsburgh, PA 15213, USA  
Prof. C. Majidi  
Department of Mechanical Engineering  
Carnegie Mellon University  
5000 Forbes Avenue, Pittsburgh, PA 15213, USA

Prof. A. W. Feinberg  
Department of Materials Science and Engineering  
Carnegie Mellon University  
5000 Forbes Avenue, Pittsburgh, PA 15213, USA

 The ORCID identification number(s) for the author(s) of this article can be found under <https://doi.org/10.1002/adhm.201901735>

DOI: 10.1002/adhm.201901735

saturation (SpO<sub>2</sub>) to determine physiologic status for diagnosis and decision making. In critical care, this includes continuous monitoring of neonates, postoperative patients, and those with cardiopulmonary disease.<sup>[1]</sup> However, current devices are rigid, bulky and burdensome to wear for long-term monitoring, which has limited their use outside the hospital for preventive care, health tracking, and the management of chronic disease.<sup>[2]</sup> This is especially a concern for diseases such as diabetes with a risk of neuropathy and peripheral arterial disease, which can lead to loss of blood flow in the limbs and ultimately amputation.<sup>[3]</sup> The emergence of consumer-grade wristband activity trackers (e.g., Apple Watch, FitBit) has also demonstrated the value of continuous monitoring of heart rate and SpO<sub>2</sub>, which has driven the advance of wearable technology including reduced battery size,<sup>[4]</sup> wireless operation,<sup>[5]</sup> continuous measurement,<sup>[6]</sup> and elimination of motion-induced artifacts.<sup>[7]</sup> This one-size-fits-all approach, however, has proved challenging to implement for long-term

medical monitoring, where there is need to fit patient-specific anatomy and record high-quality and repeatable measurements. Further, current pulse oximeter devices on the market are limited to a few anatomic locations, such as the clip-on pulse oximeter for the finger, which cannot provide information on localized perfusion in other areas of the body. The need to fabricate custom-fit medical wearables has spurred interest in advanced manufacturing methods that enable iterative design and low-cost customization.<sup>[8]</sup>

3D printing is uniquely positioned to fabricate a wearable device with patient-specific geometry in a single step based on a computer-aided design (CAD) model from anatomical scans. However, standard polymeric materials such as polylactic acid (PLA), acrylonitrile butadiene styrene (ABS), and thermoplastic polyurethane (TPU) elastomer are up to four orders of magnitude stiffer than soft tissue.<sup>[9]</sup> Using these leads to a rigid and bulky interface that is uncomfortable for long term wear and restricts movement because of the mechanical mismatch with the skin.<sup>[10]</sup> Pulse oximeters made of rigid materials can also cause pressure ischemia and skin breakdown.<sup>[11]</sup> Softer materials with lower elastic modulus and bending stiffness, and increased stretchability that are comparable to human skin ( $E \approx 1$  MPa) are needed.<sup>[12]</sup> Silicone elastomers, in particular polydimethylsiloxane (PDMS),

can be tuned to have these properties and have been used to make wearable sensors that have been tested on users' skin.<sup>[12b,13]</sup> Keeping the sensor in place is also a challenge to ensure consistent measurements longitudinally through time and adhesives have been used for this purpose.<sup>[14]</sup> Yet, chemical adhesives can irritate or breakdown the skin over continuous measurements.<sup>[12a,13a]</sup> This suggests that a well-designed PDMS wearable could apply light pressure to maintain placement without needing an adhesive. However, to date there has not been a way to directly 3D print PDMS for this type of design where pulse oximetry is needed at peripheral sites of the body such as the foot, which are susceptible to edema and skin breakdown.<sup>[15]</sup>

In this study, we combined 3D printing of PDMS with flexible electronics to develop a Patient-specific Pulse oximeter with Pressure sensing that we call a P<sup>3</sup>-wearable. The goal was to leverage freeform reversible embedding (FRE) 3D printing to directly fabricate a PDMS cuff to fit the finger or toe, and thus demonstrate proof-of-concept production of an anatomically accurate soft wearable. FRE is an embedded 3D printing technique derived from freeform reversible embedding of suspended hydrogels (FRESH) 3D bioprinting and enables printing of soft materials such as liquid PDMS prepolymers.<sup>[16]</sup> In FRE, liquid materials are printed layer by layer within a sacrificial support bath that acts as a Bingham plastic with a yield stress. As the print nozzle moves through the bath and exerts a stress above the bath's yield stress, the support briefly liquifies, enabling the deposition of the liquid materials being printed. By optimizing the rheological properties of the bath and the ink being printed, FRE can be used to print low viscosity liquids in 3D that would otherwise flow and form a puddle on the build platform. Using FRE printing of PDMS, we developed a sizing analysis framework to assess the dimensional accuracy of P<sup>3</sup>-wearable cuffs for the hand and foot based on patient measurements, and analyzed device performance. As proof-of-concept, the P<sup>3</sup>-wearable device was tested at rest, while sitting and during walking. The results demonstrate the ability to track activity, pulse, and oxygen saturation, showing the potential to continuously monitor peripheral blood perfusion.

## 2. Results

The P<sup>3</sup>-wearable was first developed for the hand and the soft PDMS cuffs were subject to a sizing analysis to determine dimensional accuracy of the printing process. The purpose of the finger cuff was to validate that we could fabricate a complete and functional P<sup>3</sup>-wearable and assess print fidelity and reproducibility. While this is a simple cylindrical shape that could be easily molded, it serves as a basic design for validation before proceeding to more complex patient-specific prints. **Figure 1a** depicts the design of the P<sup>3</sup>-wearable, starting from i) measurement of the finger, ii) FRE printing of the PDMS cuff, iii) integration of the flexible printed circuit board (fPCB) (Figure S1, Supporting Information) with the PDMS cuff, and iv) testing of the P<sup>3</sup>-wearable on the finger. First, finger measurements made with a caliper were used to design a patient-specific CAD model for 3D printing, into which a window cutout was designed as a place to insert the fPCB with the pulse oximeter and pressure sensor chip. FRE printing enabled the fabrication of the PDMS cuff with a well-defined window cutout into which the fPCB was easily integrated

using a silicone adhesive (Figure 1b). This was done purposefully because we wanted to 1) have a CAD design that minimized the total number of fabrication steps and 2) avoid additional postprocessing that would be required to cut out the window manually.

The CAD model was then scaled linearly to produce slightly different sizes, FRE printed in PDMS, and the dimensional accuracy of each cuff size was compared with the CAD model counterpart (Figure 1c). The error between the CAD model and the actual print dimensions was found to increase linearly with cuff size. The print height (z-axis) was larger than the CAD model while the inner major and minor axes (xy plane) were smaller. This makes sense because the g-code generated from the CAD model outlines a path for the center of the PDMS filaments to be printed, and the 17-gauge needle has an inner diameter of 1.219 mm, which should result in increased height and decreased inner diameter. A similar analysis was done for the window cutout designed to fit the fPCB, which had a smaller height and larger width than the CAD model (Figure 1d). There was no change as a function of overall cuff size because the window cutout dimensions were kept constant. The decrease in height was expected due to the filament diameter and the g-code pathing, however the larger width was likely due to the challenge of starting and stopping the flow of a relatively viscous print material like PDMS. Having quantified the difference in dimensions between the CAD design and the actual printed PDMS cuff, linear correction factors were used to produce a final print of a desired size.

The complete P<sup>3</sup>-wearable consists of the soft PDMS cuff integrated with the fPCB and battery and was first tested on the index finger in various sizes to determine the impact of fit on performance (**Figure 2a**). We previously reported the elastic modulus of FRE 3D printed PDMS as  $1.2 \pm 0.1$  MPa and showed that the layers have excellent fusion and can withstand tensile strain up to 130% elongation to failure, similar to cast PDMS.<sup>[16b,17]</sup> The waveforms recorded by the pulse oximeter optoelectronics and pressure sensor were output wirelessly in real time to a tablet computer (Figure 2b,c; Figure S2a,b, Supporting Information). The P<sup>3</sup>-wearable photodetector successfully recorded optical signals from the LEDs (Figure 2b; Figure S2a, Supporting Information) as well as pressure changes (Figure 2c; Figure S2b, Supporting Information). The size of the PDMS finger cuff was then linearly scaled by small percentage increments to determine the impact of fit on the optical and pressure signals (Figure 2d,e). These results for pressure due to the heartbeat and photoplethysmography (PPG) (Figure 2d,e) show that the 100% cuff has reduced signal amplitudes, which suggests this smaller size is restricting blood flow (i.e., volume) into the finger. For the larger 105% and 110% cuffs, the reduced contact force with the skin (Figure 2f) also results in decreased signal amplitudes for pressure due to the heartbeat and PPG (Figure 2d,e). The pressure amplitudes for the heartbeat for the 102% finger cuff ( $\approx 1.1$  kPa) were nearly fourfold higher than the 105% finger cuff ( $\approx 0.3$  kPa) size (Figure 2d) and were generally in sync with the PPG amplitude with respect to trends across cuff sizes (Figure 2e). Next, the contact pressure of the finger on the pressure sensor was evaluated and found to have a trend whereby it decreased as the finger cuff size increased (Figure 2f). Importantly, a statistically significant decrease in contact pressure resulted when going from the 102% to 105% finger cuff sizes, which also corresponded to the drop in pressure amplitude for the heartbeat (Figure 2d).

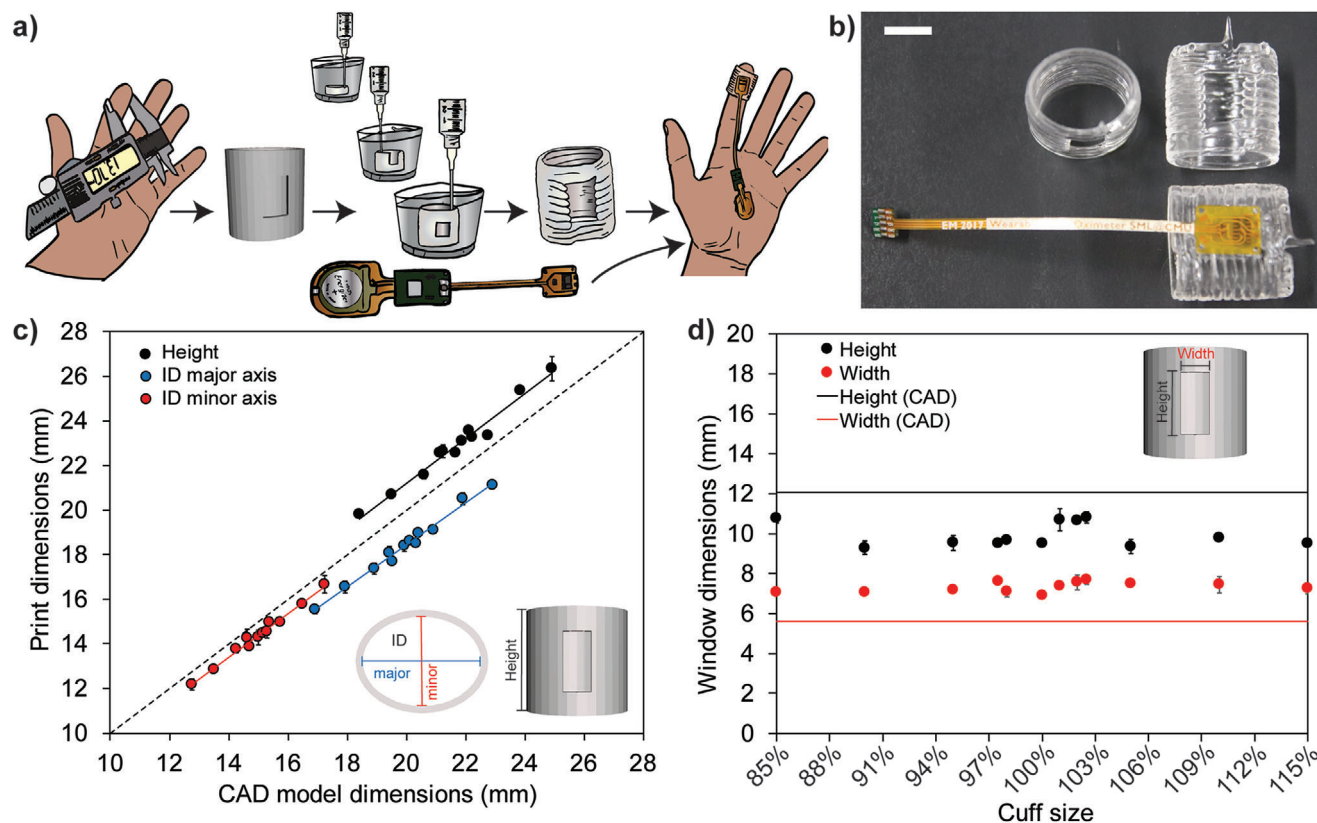


**Figure 1.** 3D printing of PDMS finger cuff for the P<sup>3</sup>-wearable device. a) Schematic of the entire process that shows i) the use of a digital caliper to take measurements on the patient's finger, ii) the design of a CAD model for the finger cuff based on the measurements, iii) the 3D printing of the finger cuff with PDMS using the FRE technique, iv) the integration of the fPCB into the PDMS finger cuff, and v) the P<sup>3</sup>-wearable worn on the hand to record pulse rate, SpO<sub>2</sub>, and pressure measurements. The fPCB for the P<sup>3</sup>-wearable includes the pulse oximeter chip (MAX30102, Maxim Integrated) with IR, and red LEDs, a barometric chip for pressure sensing, a Bluetooth low energy wireless module, and a coin cell battery. b) Examples of the 3D printed PDMS finger cuff (top view and front window view) and the PDMS finger cuff integrated with the fPCB without the battery attachment. Scale bar is 1 cm. c) Comparison of print dimensions of the 3D printed PDMS finger cuff as a function of the CAD model dimensions for different sizes (85%, 90%, 95%, 97.5%, 98%, 100%, 101%, 102%, 102.5%, 105%, 110%, and 115%) ( $n = 3$  per size). The linear fits are  $y = 1.01x + 1.06$  ( $R^2 = 0.97$ ) for the height,  $y = 0.94x - 0.48$  ( $R^2 = 0.99$ ) for ID major axis, and  $y = 0.97x - 0.24$  ( $R^2 = 0.98$ ) for ID minor axis. d) Dimensional analysis of the internal window cutout in the PDMS finger cuff compared to the CAD dimensions (5.61 mm × 12.06 mm) ( $n = 3$  per size).

This suggests that the finger cuff size of 102% gave the highest PPG and pressure amplitude for the heartbeat because there is a minimum contact pressure for reading the heartbeat through the pressure sensor, but too much contact pressure actually reduces blood flow and thus degrades the signals. Still, the difference in PPG amplitude between the 100% and 102% cuff are noteworthy (Figure 2e) even though the contact pressures are within the measurement error (Figure 2f). This is because the contact pressure is the pressure applied to the sensor, and thus only an approximate indicator of the pressure that the cuff exerts around the entire finger. Indeed, comparing PPG amplitude to contact pressure for the 100% to 110% finger cuff sizes suggested that contact pressures in the 2.5–15.5 kPa range were in the optimal range (Figure 2g). Overall, these results enabled us to understand the relationship between size and contact pressure on heartbeat amplitude and PPG amplitude, enabling us to identify a 102% finger cuff size as the best choice in this specific example.

The approach used to develop the P<sup>3</sup>-wearable for the foot was similar to the finger, except the anatomy of the toe was captured using a 3D laser scanner instead of measured using

calipers (Figure 3a). At first, the CAD model was designed with the window cutout for the pulse oximeter fPCB on the toenail for comfort and to avoid excessive pressures on the pressure sensor (Figure 3b). The 3D model generated for the big toe was more complex than the simple cylinder used for the finger and contained anatomical detail such as the toenail (Figure 3c). More complex FRE prints with overhangs and large internal voids that are challenging or impossible to 3D print in air or mold were also created in PDMS to show the versatility of the approach, including scanned models of the human face and additional models of the toe (Figure S3, Supporting Information). FRE printing produced a PDMS toe cuff with a cutout for mounting the pulse oximeter and pressure sensor chip and was able to recreate the shape of the CAD model (Figure 3d). To assess dimensional accuracy of the printed toe cuff, we scanned it using the same 3D laser scanner used to originally scan the toe and generated a 3D model (Figure 3e). We performed quantitative gauging by comparing the two CAD models and creating a heat map showing deviation of the toe cuff superimposed on the toe (Figure 3f). There were clear differences on the nail

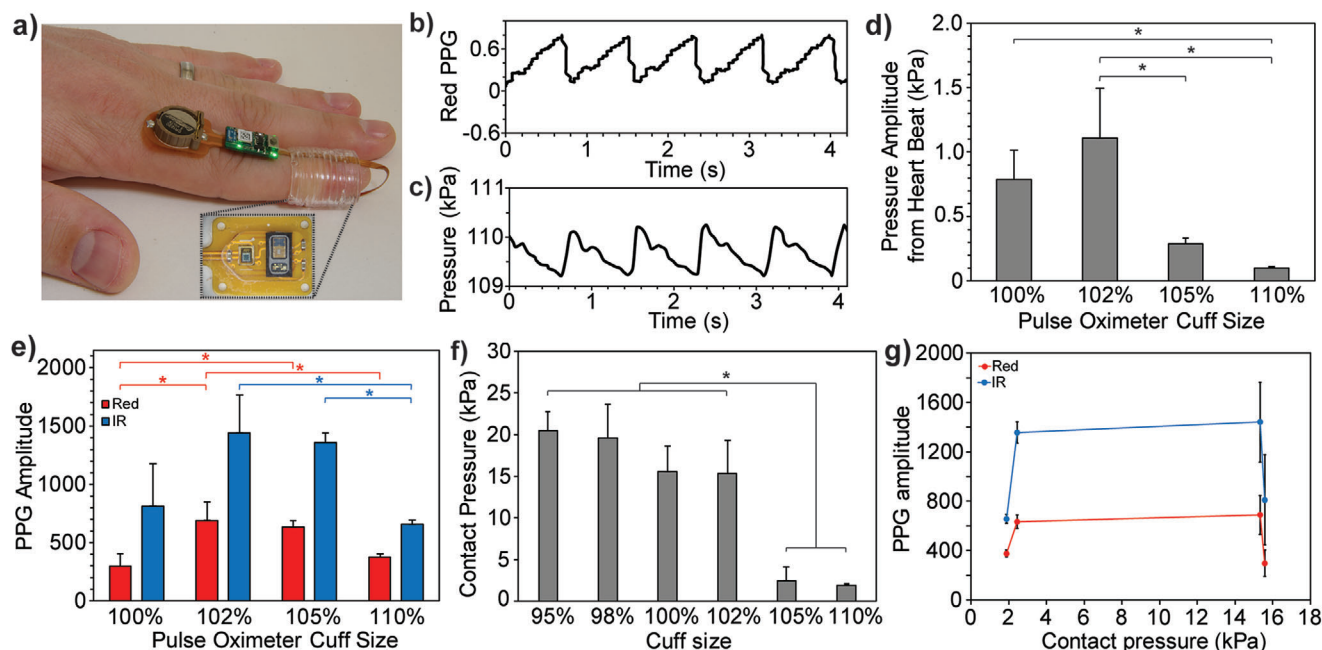


**Figure 2.** Performance of the 3D printed wearable pulse oximeter for the finger. a) Representative image of the patient-specific wearable pulse oximeter tested on the index finger. b) Raw signal output of the red PPG waveform from the pulse oximeter shows the ability to read from the finger and overall system performance with data transmitted wirelessly to the tablet computer for collection. c) Raw signal output of the pressure sensor, which is the sum of the noncontact pressure, contact pressure, and pressure from the pulsatile blood flow. d) Average amplitude of the pressure signals from the pulsatile blood flow due to the heartbeat (i.e., oscillating waveform in panel (c)) as a function of cuff size. Statistically significant differences indicated by \* ( $P < 0.05$ ) by one-way ANOVA followed by a Tukey–Kramer post hoc test ( $n = 3$ ). e) Average amplitude of the PPG from the red and IR LEDs. Statistically significant differences indicated by \* ( $P < 0.05$ ) by one-way ANOVA followed by a Tukey–Kramer post hoc test ( $n = 3$ ). f) The contact pressure between the finger and the pressure sensor as a function of cuff size. Statistically significant differences indicated by \* ( $P < 0.05$ ) by one-way ANOVA followed by a Tukey–Kramer post hoc test ( $n = 3$ ). g) Pulse oximeter PPG signal amplitude as a function of the different contact pressures applied by cuff sizes 100%, 102%, 105%, and 110% ( $n = 3$ ).

region, surrounding the pulse oximeter window, and more evenly spread throughout the cuff. However, throughout the entire toe cuff these differences were less than 2 mm, and the average deviation was less than 1 mm, with multiple prints of the same size showing similar dimensions Table S1 (Supporting Information). The dimensional accuracy across different cuff sizes from 90% to 110% were overall quite similar, providing confidence that the toe cuff can be F3D printed using PDMS with predictable dimensions (Figure S4, Supporting Information). The cuffs were then integrated with the pulse oximeter fPCB to make the complete P<sup>3</sup>-wearable for the foot (Figure 3b), which was tested in the same three step sequence (detached–worn–detached) as for the hand. Given the shape of the large toe, we decided to evaluate the P<sup>3</sup>-wearable with the fPCB located in three different positions; on the top of the toenail, on the bottom of the toe and on the side of the toe (Figure 3a).

Results showed that there were clear differences based on the cuff size and the location of the sensor on the toe (Figure 3g–i). However, a change in the size and location did not necessarily result in a similar change to both the PPG and pressure signals. For example, the 95% and 100% cuff sizes on the nail (top) and beneath the toe (bottom) had overall higher PPG amplitudes. In contrast, a much smaller cuff size of 83% with the sensor on the side of the toe also had both high PPG and pressure signals, but other sizes with the sensor on the side (78%, 80%, 85%, and 100%) either did not fit (i.e., too small to wear) or had very low

signal, and thus none of these sizes were further analyzed. Additionally, when the sensor was placed beneath the toe (bottom), the PPG amplitude for the red LED was overall higher than on the nail (top) (Figure 3g). Yet the pressure amplitude for the 90% cuff size was larger with the sensor placed on the nail (top) versus beneath the toe (bottom) (Figure 3i). Taken together, these results highlight the fact that cuff size and location impact the P<sup>3</sup>-wearable's functional performance and that all locations (e.g., bottom, top, and side) have the potential to work. Based on the results though, we identified the 90% toe cuff size with the sensor on the nail (top) as the best option for recording both the PPG and pressure signal from the heartbeat. There are also other variables such as the wavelength of light, the anatomical location, and the proximity of the arteries to the surface of the skin that are a determinant of the output signal. Thus, customization may be necessary depending on the sensitivity needed for a given application.

Finally, we evaluated the performance of the P<sup>3</sup>-wearable in various usage scenarios with the 90% toe cuff size and the fPCB integrated on the nail in order to minimize direct pressure being placed on the fPCB electronics. The P<sup>3</sup>-wearable was tested at rest with the foot extended flat and without putting any weight on the device (Figure 4a), and then compared to sitting (Figure 4b) and walking (Figure 4c) (note that the battery and Bluetooth module were on top of the foot). The signal recordings during the at rest and sitting conditions had the typical pulsatile waveforms for the

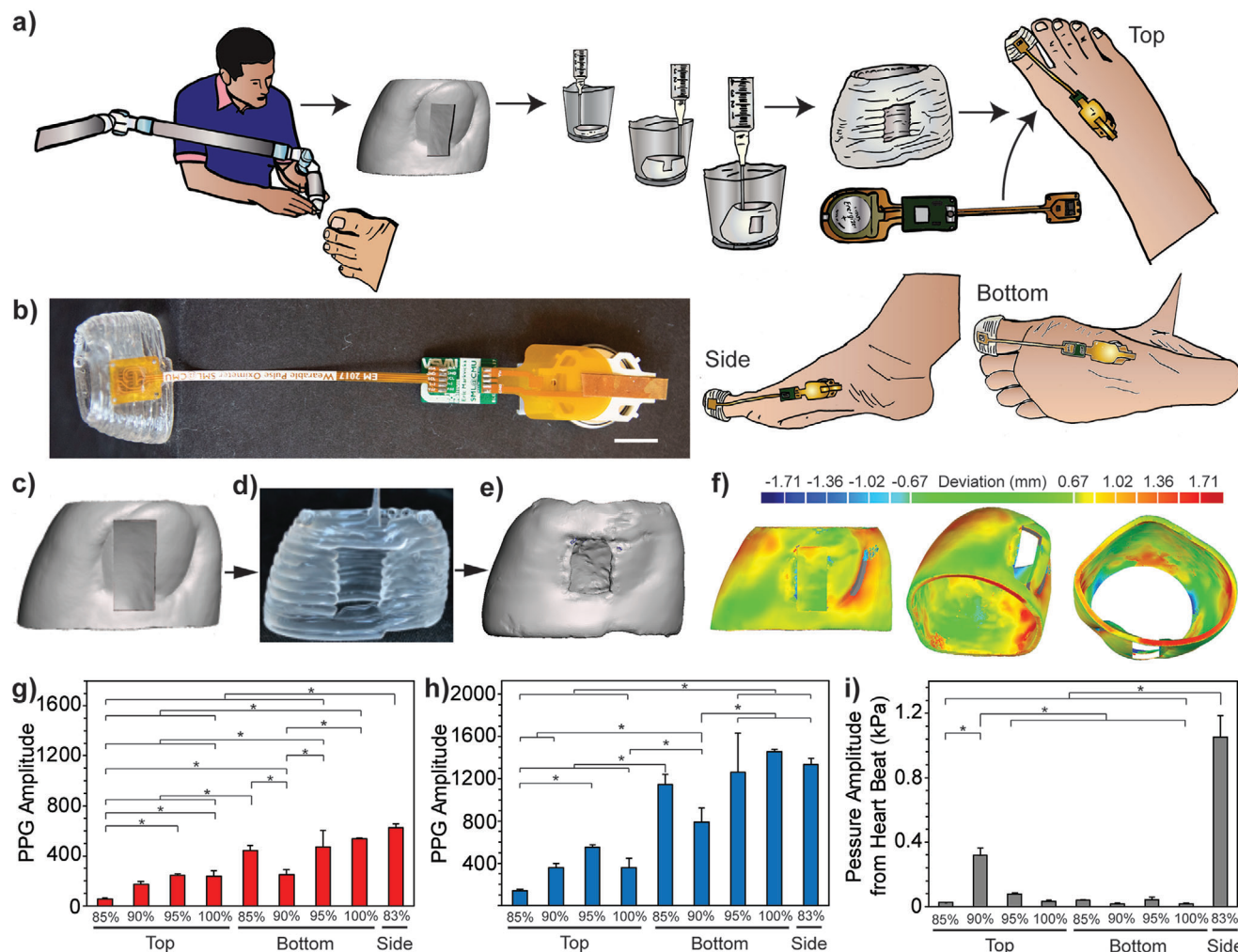


**Figure 3.** Fabrication, assessment and performance of the 3D printed wearable pulse oximeter for the toe. a) Schematic of the fabrication process showing i) 3D scanning of the patient's toe, ii) generation of a CAD model of the toe cuff based on the scan, iii) 3D printing the toe cuff with PDMS using the FRE technique, iv) integrating the fPCB with pulse oximeter chip into the PDMS toe cuff, and v) wearing the completed sensor on the toe to record pulse and SpO<sub>2</sub>, with the chip positioned on the top, bottom or side of toe. b) Complete wearable toe pulse oximeter with the pulse oximeter window placement on the bottom of the toe. Scale bar = 1 cm. The fPCB includes the pulse oximeter chip (MAX30102, Maxim Integrated) with IR and red LEDs, a barometric chip for pressure sensing, a Bluetooth low energy wireless module, and a coin cell battery. c) CAD model for 3D printing the toe cuff obtained from the 3D anatomical scan. d) Toe cuff 3D printed from PDMS using the FRE technique. e) CAD model of the printed PDMS toe cuff obtained by 3D scanning of the printed toe cuff in (d). f) Quantitative gauging analysis showing the deviation of the CAD model for the toe cuff compared to the CAD model from the scan of the printed PDMS toe cuff with the color code indicating the differences between the two. g) Signal amplitude for the red LED of the pulse oximeter as a function of cuff size and location. One-way ANOVA was used to determine statistical significance followed by a Tukey–Kramer post hoc test indicated by \* ( $P < 0.05$ ,  $n = 3$ ). h) Signal amplitude for the IR LED of the pulse oximeter as a function of cuff size and location. One-way ANOVA was used to determine statistical significance followed by a Tukey–Kramer post hoc test indicated by \* ( $P < 0.05$ ,  $n = 3$ ). i) Signal amplitude for the pressure from the pulsatile blood flow as a function of cuff size and location. One-way ANOVA was used to determine statistical significance followed by a Tukey–Kramer post hoc test indicated by \* ( $P < 0.05$ ,  $n = 3$ ).

foot red and IR PPG, and pressure (Figure 4a,b). However, there was a marked decrease in the signal amplitude sitting compared to at rest. As seen for the finger, the peaks of the cyclical pressure recordings for both conditions (Figure 4a,b) were inversely correlated to the PPG signal. The heart rate and SpO<sub>2</sub> calculated from the PPG signals recorded by the P<sup>3</sup>-wearable matched values obtained with a commercial pulse oximeter worn at the same time on the index finger. At rest, the P<sup>3</sup>-wearable recorded SpO<sub>2</sub> of 100% and heart rate of 63 beats min<sup>-1</sup>, while the commercial pulse oximeter recorded SpO<sub>2</sub> of 98% and 64 beats min<sup>-1</sup>.

While sitting, the P<sup>3</sup>-wearable recorded SpO<sub>2</sub> of 98% and heart rate of 71 beats min<sup>-1</sup>, while the commercial pulse oximeter recorded SpO<sub>2</sub> of 97% and 71 beats min<sup>-1</sup>. While these values could be quantified for the at rest and sitting conditions, walking resulted in large increases in the pressure and large decreases in the PPG signals (Figure 4c). During the period of contact of the foot with the ground, the pressure signal increased by 5–10 kPa over baseline, obscuring any pulsatile signal from blood the flow, and corresponded to a decrease in the PPG signals. While the PPG signals increased and the pressure decreased during the

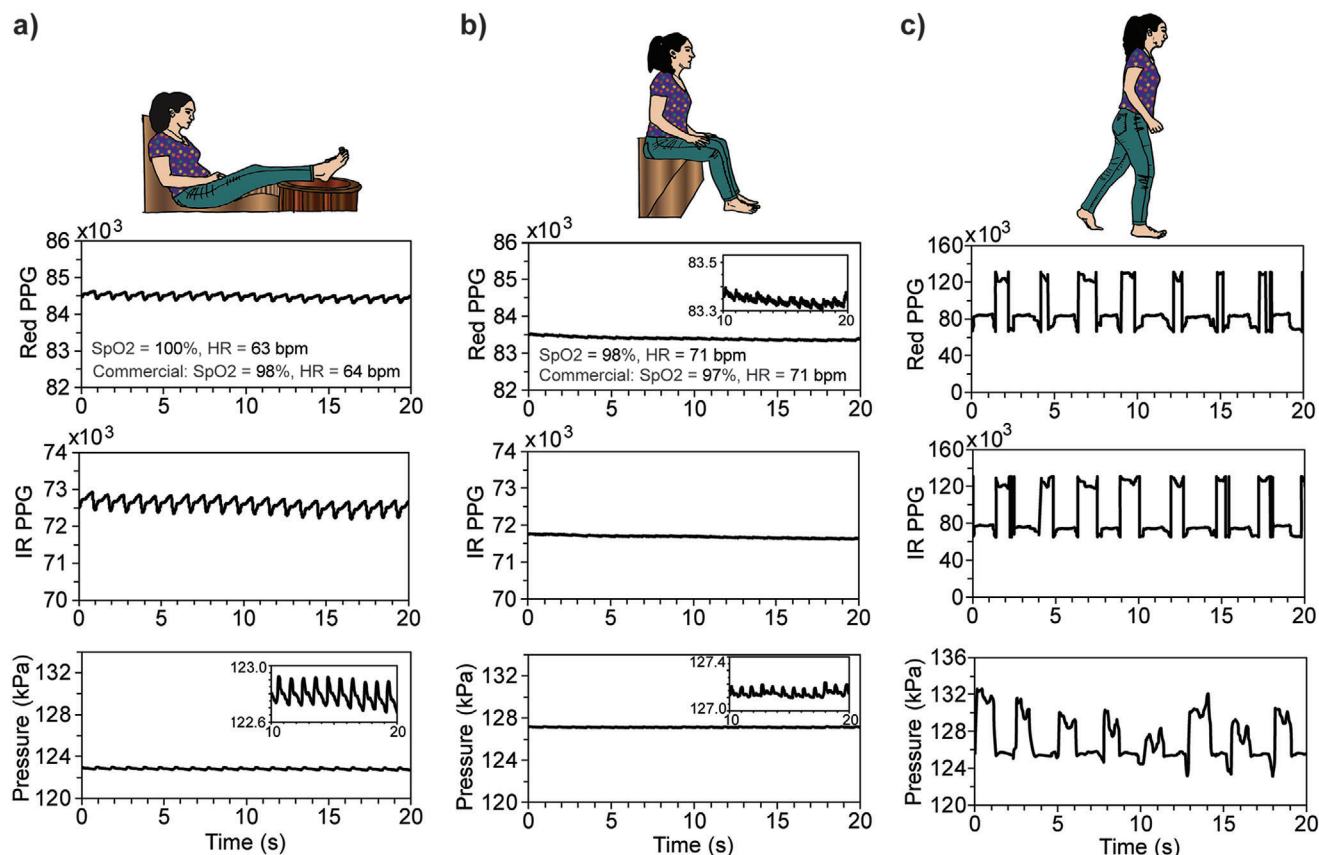


**Figure 4.** Activities testing with the 90% cuff wearable pulse oximetry on top of the toenail. The three states of pulse oximeter signal recording of the Red PPG, IR PPG, and contact pressure during wear are a) at rest (no weight), b) sitting, and c) walking.

noncontact phase of the gait cycle, oscillations remained and neither produced a usable signal. It is thought that this was due to movement of the fPCB relative to the toe, producing motion artifacts. While not usable during walking, the signals from the P<sup>3</sup>-wearable could easily be used to determine when the user is moving and restrict reading of usable PPG and pressure signals to periods of rest or sitting. Further studies are needed to assess the comfort of the device for long term wear and will ultimately be part of product development if commercialized.

### 3. Discussion

The P<sup>3</sup>-wearable we have developed has its basis in the ability to 3D print PDMS elastomer using the FRE process to create a patient-specific soft cuff. However, FRE is a recently developed approach and there has been limited data on dimensional accuracy.<sup>[16a-e]</sup> Like most 3D printing,<sup>[18]</sup> there are many print parameters such as speed, flowrate, and layer height that have an effect on the dimensions of the PDMS cuffs relative to the CAD model. Here, we selected these parameters based on our previously published Expert Guided Optimization approach.<sup>[17]</sup> Our results found that the absolute mean deviation of the PDMS prints compared to the CAD model did not exceed 1 mm for the finger (Figure 1c) or the toe cuffs (Figure S4 and Table S1, Supporting Information). The sizing analysis found linear cor-

rection factors for the finger cuff, but these likely cannot be universally applied to other sizes and shapes, in part because of differences in the way initial anatomical measurements are made. Still, the correction factors provide a starting point, and the print dimensions may be within a clinically acceptable range depending on the application. For example, Ashtiani et al. reported that 3D printed dental onlays, compared to onlays made with conventional methods, were within the clinically acceptable marginal discrepancy (20–150  $\mu\text{m}$ ) for this application.<sup>[19]</sup> In another study on an ear prosthesis, the clinically acceptable mean difference between the printed prosthesis and the subject was reported as 2 mm (1.5%).<sup>[20]</sup> Thus, our average difference between the prints and digital cuff dimensions may be within the clinically acceptable range for a wearable pulse oximetry application.

Overall, differences across the signal amplitudes of the PPG and pressure sensors revealed that both the location of the sensors and the size of the cuff affect the device's performance (Figures 2d,e and 3g–i). The PPG signal oscillations resulted from changes in blood volume during the systolic and diastolic phases of the cardiac cycle, and the pressure sensor was able to detect the same changes. Having tested different cuff sizes provided a means to study the effect of contact pressure on signal amplitudes (Figure 2f,g). Contact pressures in the 2.5–15.5 kPa range that corresponded to 102% and 105% cuff sizes were found to have the largest amplitudes (Figure 2g). Dresler and Mendelson found a similar pressure range of 8–12 kPa was optimal to obtain

higher PPG amplitudes.<sup>[7a]</sup> In the latter study, the contact pressure was changed crudely by pressing on the sensor, however, the results corroborated our findings on the implications of cuff fit on device performance.<sup>[7a]</sup> Additional studies will be required to assess the effect of anatomic shape and sensor location on signal quality.

The PPG and pressure signals were different through each activity (at rest, sitting, and walking) when testing the P<sup>3</sup>-wearable on the toe with the fPCB on the nail in the 90% cuff size (Figure 4). The signal when sitting was smaller than at rest likely because the pressure exerted by the ground on the bottom of the toe deformed the PDMS cuff and slightly decreased fPCB contact with the nail. Still, both at rest and sitting, the P<sup>3</sup>-wearable produced usable signals to extract the heart rate and blood oxygen content. The calculated values were comparable to the output from a commercial oximeter worn simultaneously on the index finger with a  $\pm 2\%$  accuracy (Figure 4a,b).<sup>[21]</sup> The signal recordings when walking could not be used due to motion artifacts as the foot was lifted and then the foot hit the ground. This caused a change in pressure in the toe and thus the amount of blood volume as well as contact with the sensor. However, for our purpose we do not need to be continually reading SpO<sub>2</sub>, and taking measurements even as infrequently as once per hour during short periods of rest is adequate. In this case the distinctive shape of the pressure and PPG signals were indicative of walking and together inform on patient activity status. Future iterations of this device could automatically determine the activity state from the PPG and/or pressure signal and then only calculate heart rate and blood oxygen content during sitting or rest states.

We will need to perform longer term studies to evaluate performance of the P<sup>3</sup>-wearable and any impact on the skin over time. The benefit of a customized cuff over a bandage lies in avoiding direct contact of the skin with chemical adhesives, which can cause irritation and increase risk of infection in patients with ulcers, sensitive skin, and other complications. Similarly, the benefit of a customized cuff over a molded rubber band-type cuff is the ability to tailor to the anatomical shape of the body in order to minimize pressure points while maintaining adequate signal. We recognize that traditional molding techniques remain feasible to produce soft wearable cuffs of different sizes in limited geometries. Future work should thus look toward assessing this (molding versus 3D printing) and other competing technologies through cost-benefit analysis to determine the most suitable for a given application. Additionally, for the P<sup>3</sup>-wearable we will need to perform long term testing of durability and on a wider number of users as the device moves toward commercialization.

## 4. Conclusion

In this study, the P<sup>3</sup>-wearable was developed by combining FRE 3D printing of PDMS with a pulse oximeter and pressure sensor chip on an fPCB. Pulse oximetry noninvasively measured blood oxygenation and pulse rate by relying on the optical detection of volume changes in blood vessels. Traditionally, in the clinic a one-size-fits-all rigid device such as a finger clip is used for short-term monitoring. In contrast, the P<sup>3</sup>-wearable is wireless, small sized ( $\approx 8$  cm), provides continuous real-time feedback on a tablet, and made from soft and flexible materials throughout. Further, we in-

roduced a workflow to match the design to different anatomical locations, which can serve as a model for potential clinical implementation. This approach can also be used to determine the implications of patient matching on the device performance. Looking forward, the P<sup>3</sup>-wearable can be improved with additional sensors, for example an accelerometer, to better track patient activity. Though designed for the finger and toe, this approach may be adapted for sensors in other anatomic locations. In addition, future testing of the P<sup>3</sup>-wearable should be done with a sample population to evaluate the ability to conform to variable anatomy between individuals. Ultimately, commercial translation will require meeting the U.S. Food and Drug Administration (FDA) guidelines on the requirements for receiving a 510(k) approval to market oximeters as a medical device.

## 5. Experimental Section

*Freeform Reversible Embedding (FRE) 3D Printing of Silicone Process and Preparation:* The FRE 3D printing process has been previously described.<sup>[16b,17]</sup> Briefly, a fused deposition modeling (FDM) 3D printer, used to 3D print standard filament-based thermoplastics, was modified to 3D print liquid silicone. The modification involved using the 3D printer to build a syringe-based extruder that then served to replace the original extruder on the Makerbot Replicator dual 3D Printer (Makerbot Industries, LLC, NY). Aside from hardware modification, FRE involved 3D printing within a sacrificial support bath to sustain the build of liquid layers from the bottom up. The support bath was a yield stress fluid, the polyacrylic acid microgel Carbopol 940 (Lubrizol Corporation, OH) at 2% w/v. The bath was prepared by first mixing Carbopol 940 in deionized water and thereafter neutralizing the solution to pH  $\approx 7$  by adding sodium hydroxide. The silicone elastomer used for 3D printing was Sylgard 184 (Dow Corning Corporation, MI), the preparation of which required mixing a two-component base-to-catalyst at a 10:1 ratio by weight. Both bath ( $\approx 75$  g) and the silicone were mixed prior to use for 2 min in a Thinky-Conditioning planetary centrifugal mixer (Phoenix Equipment Inc, NY) and then defoamed for another 2 min at 2000 RPM. The silicone was loaded into the syringe-based extruder of the 3D printer and extruded through a 17-gauge needle with a 1.219 mm inner diameter (Jensen Global Inc, CA) and then inserted into the cup containing the bath that was placed onto the print platform. The 3D printing software Simplify3D (Simplify3D, OH) was used and the code was customized to complement the syringe-based 3D printing process. Each cuff printed in less than 2 min, after which the print container was placed in an oven at 65 °C to heat cure the PDMS for 2 h. After this the printed cuff was manually removed from the Carbopol support bath and then briefly washed off with water to remove any loosely adhered bath residue.

*Finger Cuff Design, Sizing, and 3D Printing:* The dimensions of the distal phalanx segment of a person's index finger (major axis = 17.9 mm; minor axis = 13.7 mm; height = 23 mm) was measured with a digital caliper at the widest point for the width (major axis) and thickness (minor axis). The measurements were then used to design a cylindrical shaped cuff CAD model. The CAD was also designed with a window to the size of the pulse oximeter chip (6.35 mm width  $\times$  10.55 mm height) that was measured using a caliper. The CAD model as is and with the pulse oximeter window were 3D printed in silicone (Sylgard 184). A sizing analysis was performed to determine and compare the dimensional accuracy of the prints relative to the CAD models. The relative mean difference between the silicone cuff and the CAD model from the sizing analysis was then used as correction factors (5.77% height, -9.49% ID minor axis, and -11.28% ID major axis) to design the final finger cuff CAD model (height = 21.67 mm; ID major axis = 19.92 mm; ID minor axis = 15 mm). Similarly, correction factors for the pulse oximeter window (width = 18.67%; height = -14.3%) based on the relative mean difference between the silicone print and the CAD were used to design the final CAD window (width = 5.61 mm; height = 12.06 mm; note: the corrected width is slightly smaller than the 18.67%

correction factor). The final CAD model dimensions was thenceforth used as the reference size model, 100% to the dimensions of the finger, which served as basis to create other CAD sizes both smaller and larger (85%, 90%, 95%, 97.5%, 98%, 101%, 102%, 102.5%, 105%, 110%, and 115%). The window dimensions across CAD sizes were kept constant because the size of the fPCB does not change. The wall thickness of all CAD models was also maintained constant at 1.2 mm, the diameter of the print nozzle throughout the study. Each CAD size was printed three times and each dimension (height, ID major and minor axes, wall thickness major and minor axes, and window width and height) was measured three times by a caliper ( $n = 108$ ). All CAD models were designed using the Meshmixer (Autodesk, Inc.) software and 3D printed with the Simplify3D (S3D) software (extrusion multiplier = 1.4).

**Toe Cuff Design, Sizing, and 3D Printing:** A patient-specific CAD model of the toe was developed by scanning a cast of a toe using the NextEngine Desktop 3D scanner (NextEngine, Inc.). The cast was made from plaster using the Lifecasting Alja-Safe Starter Kit (Smooth-On, Inc.). Briefly, the first step involved creating the Alja-Safe molding gel that required mixing the Alja-Safe powder with water at a 1:1 mixing ratio by volume. The toe was inserted into the gel and left in for the gel to set for 8–10 min. Subsequent removal of the toe produced a toe-shaped mold cavity for casting with plaster. The plaster was prepared by mixing with water at a 2:1 ratio by volume. After pouring into the mold, the plaster was left to cure for  $\approx 3$  h. The life-size toe cast was scanned, repaired and then processed with a combination of software that include ScanStudio (NextEngine, Inc.), Netfabb (Autodesk, Inc.), and Meshmixer (Autodesk, Inc.). The CAD model was then offset to have a 1.2 mm wall thickness. The top of the toe was cut from the CAD model mainly to avoid nonadhering silicone layers during 3D printing that resulted from the reduction in layer dimensions and for potential comfort. To adjust for the dimensional accuracy of the prints, the correction factors found from the finger cuff sizing analysis (5.77% height; -9.49% ID minor axis; -11.28% ID major axis) were used in the sizing of the toe cuff CAD model. This CAD was considered the model to the dimension of the toe that is the 100% size. This and other CAD sizes were made with the window placed on the nail (85%, 90%, 95%, 100%, 102.5%, and 105%), beneath (85%, 90%, 95%, 97%, and 100%), and to the side (78%, 80%, 83%, 85%, and 100%) of the toe. The pulse oximeter window was the same size as the fPCB previously measured and designed on the finger cuff (width = 5.61 mm; height = 12.06 mm). The toe was printed in silicone (Sylgard 184) using the S3D software with an extrusion multiplier of 2 to achieve layer adhesion.

**Assessing the 3D Printed Toe Cuff Dimensional Accuracy Relative to the CAD Model:** The dimensional accuracy of the printed cuffs was assessed by a surface area and a deviation analysis with the original and a CAD model obtained by scanning the prints. This was done for nine cuff sizes (90%, 95%, 97.5%, 100%, 102.5%, 105%, and 110%) with the pulse oximeter window designed on the nail. The reverse engineering of the 3D prints ( $n = 2$ ) was performed using the FARO ScanArm laser scanner (FARO Technologies, Inc.) for all sizes. The wall thickness of the printed toe was captured by scanning both the inside and outer surface. The deviation, in millimeters, between the CADs was determined by first aligning the two models using the Geomagic Wrap (3D Systems, Inc.) software. A best-fit alignment was used with 1500 sample size and high precision fitting. Subsequently, the built-in deviation analysis of Geomagic was used with the original CAD set as the reference model. The surface area of each model was determined through the Geomagic surface area analysis feature.

**Pulse Oximetry and Pressure Sensing Wearable Fabrication, Testing, and Data Processing:** A flexible printed circuit board (fPCB) harboring the pulse oximetry and pressure sensor capability was developed (Figure S1, Supporting Information) using a fabrication technique described recently.<sup>[22]</sup> Briefly, a UV laser micromachining system was used to pattern and assemble soft layers and rigid parts such as polyacrylic acid elastomer and the pressure sensor, respectively. The MEMS piezoresistive pressure sensor was commercially available, the barometer cover was removed and embedded in the elastomer. The reflectance pulse oximeter sensor was also commercially available (MAX30102, Maxim Integrated) and the chip contained a red LED (660 nm), infrared LED (880 nm), a photodetector, and analog signal processing. The fPCB was inserted into

the patient-matched silicone cuff and held in place by friction fit, using the silicone-based adhesive Sil-Poxy (Smooth-On, Inc.) on the cuff window brims. Each wearable was tested in three stages (Figure S2, Supporting Information) that recorded while 1) detached and on a table ( $\approx 30$  s), 2) worn on the finger or toe ( $\approx 60$ – $90$  s), and again 3) detached and on a table ( $\approx 30$  s). The data collected at a sampling frequency of 100 Hz was transmitted wirelessly at 15 Hz to a tablet via a Bluetooth low energy (BLE) module (Nordic nRF5122) powered by a lithium coin cell battery (CR1220). A graphical user interface (GUI) was developed in C# to display the PPG and pressure waveforms in real time, which were thereafter processed in MATLAB. Informed signed consent was obtained from coauthors S.A. and E.J.M. for application of the body-mounted pulse-oximetry cuff (P<sup>3</sup>-wearable), which includes the recording of PPG, SpO<sub>2</sub>, pressure, and/or any other data reported throughout all figures. For the period signals that the device was worn, the average peak amplitudes (IR PPG, red PPG, and pressure) that reflect arterial blood flow were extracted from a subset (30 s interval) of the recordings. The full detached–worn–detached recording set was used to obtain the contact pressure on the barometer. Specifically, the average pressure offset while the cuff was detached was subtracted from the average pressure while the cuff was worn ( $P_{\text{contact, toe/finger}} = P_{\text{contact, worn}} - P_{\text{contact, detached}}$ ). To calculate heart rate and arterial oxygen saturation of hemoglobin (SpO<sub>2</sub>), data were processed by applying standard feature extraction techniques. The analysis was based on the modified Beer–Lambert law.<sup>[23]</sup> Heart rate was calculated from the maximum peak between 0.8 and 1.8 Hz of a fast Fourier transform (FFT). The molar extinction coefficients for red and near-infrared light for oxyhemoglobin and deoxyhemoglobin ( $\epsilon_{660 \text{ nm, HbO}} = 0.77 \text{ mm}^{-1} \text{ cm}^{-1}$ ,  $\epsilon_{660 \text{ nm, Hb}} = 7.921 \text{ mm}^{-1} \text{ cm}^{-1}$ ,  $\epsilon_{880 \text{ nm, HbO}} = 2.957 \text{ mm}^{-1} \text{ cm}^{-1}$ ,  $\epsilon_{880 \text{ nm, Hb}} = 1.936 \text{ mm}^{-1} \text{ cm}^{-1}$ ) were obtained from.<sup>[24]</sup> The distance between the LEDs and photodetector was 3.8 mm. The ratio of differential pathlength factor (DPF), which accounts for wavelength dependent scattering differences, was set to 1.4 based on Kohl et al.<sup>[25]</sup> The SpO<sub>2</sub> is an average based on values calculated using the fast Fourier transform (FFT) and the Hilbert transform. This output was compared with a commercial oximeter, the Masimo MightySat Fingertip Pulse Oximeter (Masimo Corporation), which was worn simultaneously on the index finger.

**Statistical Analysis:** For the finger cuff design, a one-sample *t*-test ( $n = 18$ ,  $\alpha = 0.05$ ) was performed to compare the average print dimensions to the CAD model. Additionally, statistical tests were performed on the wearable hand and foot pulse oximetry signal output. Overall, the data passed the W/S normality test ( $n = 3$ ,  $\alpha = 0.05$ ) and were assumed normal. For the amplitudes of IR PPG, red PPG, and pressure from heartbeat, a one-way ANOVA ( $n = 3$ ,  $\alpha = 0.05$ ) and Tukey–Kramer post hoc test were applied separately to assess for statistical significance across the cuffs. For the finger, the cuffs were of different sizes (100%, 102%, 105%, and 110%). For the toe, the cuffs were of different sizes and placed at different locations (nail 85%, nail 90%, nail 95%, nail 100%, beneath 85%, beneath 90%, beneath 95%, beneath 100%, and side 83%). The contact pressure output that could be quantified for the hand wearable was subject to the same statistical analysis as the finger cuff sizes. The statistical analysis was performed using Microsoft Excel's Analysis ToolPak feature. The data in the figures were presented as the mean  $\pm$  the standard deviation (SD).

## Supporting Information

Supporting Information is available from the Wiley Online Library or from the author.

## Acknowledgements

The authors thank Prof. Jana Kainerstorfer for writing the MATLAB code to extract SpO<sub>2</sub> and heart rate values from raw PPG signals, Niki Abdollahi for her contributions to the activity schematics, and Andrew Holmes for providing access to the FARO ScanArm laser scanner. This work was financially supported by the Disruptive Health Technology Institute at Carnegie Mellon University (A017261-HIGHMARK-Feinberg).

## Conflict of Interest

A.W.F. has an equity stake in FluidForm Inc., which is a startup company commercializing FRE 3D printing. FRE 3D printing is the subject of patent protection including U.S. Patent 10150258 and others.

## Keywords

3D printing, health monitors, pulse oximeters, soft materials, wearable devices

Received: December 3, 2019

Revised: May 3, 2020

Published online:

- [1] J. W. Salyer, *Respir. Care* **2003**, *48*, 386.
- [2] M. Koziół, P. Piech, M. Maciejewski, W. Surtel, *Acta Angiol.* **2019**, *25*, 28.
- [3] a) N. Narula, A. J. Dannenberg, J. W. Olin, D. L. Bhatt, K. W. Johnson, G. Nadkarni, J. Min, S. Torii, P. Poojary, S. S. Anand, J. J. Bax, S. Yusuf, R. Virmani, J. Narula, *J. Am. Coll. Cardiol.* **2018**, *72*, 2152; b) H. Reinecke, M. Unrath, E. Freisinger, H. Bunzemeier, M. Meyborg, F. Lüders, K. Gebauer, N. Roeder, K. Berger, N. M. Malyar, *Eur. Heart J.* **2015**, *36*, 932.
- [4] a) Y. Mendelson, R. J. Duckworth, G. Comtois, presented at *2006 Int. Conf. on IEEE Engineering in Medicine and Biology Society*, August–September **2006**; b) M. Savage, C. Pujary, Y. Mendelson, presented at *2003 IEEE 29th Annu. Proc. Bioengineering Conference*, March **2003**; c) M. Tavakoli, L. Turicchia, R. Sarpeshkar, *IEEE Trans. Biomed. Circuits Syst.* **2010**, *4*, 27.
- [5] a) F. Adochiei, C. Rotariu, R. Ciobotariu, H. Costin, presented at *2011 7th Int. Symp. on Advanced Topics in Electrical Engineering (ATEE)*, May **2011**; b) N. Constant, O. Douglas-Prawl, S. Johnson, K. Mankodiya, presented at *2015 IEEE 12th Int. Conf. on Wearable and Implantable Body Sensor Networks (BSN)*, June 2015; c) P. B. Crilly, E. T. Arakawa, D. L. Hedden, T. L. Ferrell, presented at *IEEE Instrumentation and Measurement Technology Conference Sensing, Processing, Networking (IMTC Proceedings)*, May **1997**; d) J. W. Lebak, J. Yao, S. Warren, in *Proc. 25th Annu. Int. Conf. on the IEEE Engineering in Medicine and Biology Society*, Vol. 4, IEEE, Cancun, Mexico **2003**, p. 3196; e) M. Poh, N. C. Swenson, R. W. Picard, *IEEE Trans. Inf. Technol. Biomed.* **2010**, *14*, 786; f) J. Yao, R. Schmitz, S. Warren, *IEEE Trans. Inf. Technol. Biomed.* **2005**, *9*, 363.
- [6] a) K. Reinhart, H.-J. Kuhn, C. Hartog, D. L. Bredle, *Intensive Care Med.* **2004**, *30*, 1572; b) T. Tamura, Y. Maeda, M. Sekine, M. Yoshida, *Electronics* **2014**, *3*, 282; c) S. Warren, Y. Jianchu, G. E. Barnes, presented at *Proc. Second Joint 24th Annual Conference and the Annual Fall Meeting of the Biomedical Engineering Society (Engineering in Medicine and Biology)*, October **2002**; d) M. W. Wong, H. F. Tsui, S. H. Yung, K. M. Chan, J. C. Cheng, *J. Trauma: Inj., Infect., Crit. Care* **2004**, *56*, 356.
- [7] a) R. P. Drescher, Y. Mendelson, presented at *2006 Int. Conf. on IEEE Engineering in Medicine and Biology Society*, August–September **2006**; b) Y. Lee, S. Jung, Y. Seo, W. Chung, presented at *2008 Third Int. Conf. on Convergence and Hybrid Information Technology*, November **2008**; c) R. Sokwoo, Y. Boo-Ho, H. H. Asada, *IEEE Trans. Biomed. Eng.* **2001**, *48*, 795.
- [8] a) K. Xu, Y. Lu, K. Takei, *Adv. Mater. Technol.* **2019**, *4*, 1800628; b) Y. Huang, X. Fan, S. C. Chen, N. Zhao, *Adv. Funct. Mater.* **2019**, *29*, 1808509.
- [9] M. A. Meyers, P.-Y. Chen, A. Y.-M. Lin, Y. Seki, *Prog. Mater. Sci.* **2008**, *53*, 1.
- [10] a) L. E. Dunne, H. Profita, C. Zeagler, J. Clawson, S. Gilliland, E. Y. Do, J. Budd, presented at *2014 36th Annu. Int. Conf. on IEEE Engineering in Medicine and Biology Society*, August **2014**; b) Y. Liu, M. Pharr, G. A. Salvatore, *ACS Nano* **2017**, *11*, 9614.
- [11] a) D. Jackson, A. M. Sarki, R. Betteridge, J. Brooke, *Int. J. Nurs. Stud.* **2019**, *92*, 109; b) M. Schallom, D. Prentice, C. Sona, C. Arroyo, J. Mazuski, *Heart Lung* **2018**, *47*, 93; c) C. Ceran, O. F. Taner, F. Tekin, S. Tezcan, O. Tekin, B. Civelek, *J. Pediatr. Surg.* **2012**, *47*, e27.
- [12] a) L. Gao, Y. Zhang, V. Malyarchuk, L. Jia, K.-I. Jang, R. Chad Webb, H. Fu, Y. Shi, G. Zhou, L. Shi, D. Shah, X. Huang, B. Xu, C. Yu, Y. Huang, J. A. Rogers, *Nat. Commun.* **2014**, *5*, 4938; b) S. Harada, K. Kanoo, Y. Yamamoto, T. Arie, S. Akita, K. Takei, *ACS Nano* **2014**, *8*, 12851.
- [13] a) M. K. Choi, O. K. Park, C. Choi, S. Qiao, R. Ghaffari, J. Kim, D. J. Lee, M. Kim, W. Hyun, S. J. Kim, H. J. Hwang, S.-H. Kwon, T. Hyeon, N. Lu, D.-H. Kim, *Adv. Healthcare Mater.* **2016**, *5*, 80; b) K.-I. Jang, S. Y. Han, S. Xu, K. E. Mathewson, Y. Zhang, J.-W. Jeong, G.-T. Kim, R. C. Webb, J. W. Lee, T. J. Dawidczyk, R. H. Kim, Y. M. Song, W.-H. Yeo, S. Kim, H. Cheng, S. I. Rhee, J. Chung, B. Kim, H. U. Chung, D. Lee, Y. Yang, M. Cho, J. G. Gaspar, R. Carbonari, M. Fabiani, G. Gratton, Y. Huang, J. A. Rogers, *Nat. Commun.* **2014**, *5*, 4779; c) Y. S. Rim, S.-H. Bae, H. Chen, N. De Marco, Y. Yang, *Adv. Mater.* **2016**, *28*, 4415.
- [14] G. S. Jeong, D.-H. Baek, H. C. Jung, J. H. Song, J. H. Moon, S. W. Hong, I. Y. Kim, S.-H. Lee, *Nat. Commun.* **2012**, *3*, 977.
- [15] C. Y. L. Chao, Y.-P. Zheng, G. L. Y. Cheing, *Diabetes Technol. Ther.* **2012**, *14*, 602.
- [16] a) T. Bhattacharjee, S. M. Zehnder, K. G. Rowe, S. Jain, R. M. Nixon, W. G. Sawyer, T. E. Angelini, *Sci. Adv.* **2015**, *1*, e1500655; b) T. J. Hinton, A. Hudson, K. Pusch, A. Lee, A. W. Feinberg, *ACS Biomater. Sci. Eng.* **2016**, *2*, 1781; c) H. Kathleen, S. Bjorn, G. Christophe, L. Jared, T. Skylar, *3D Print. Addit. Manuf.* **2017**, *4*, 123; d) C. S. O'Bryan, T. Bhattacharjee, S. Hart, C. P. Kabb, K. D. Schulze, I. Chilakala, B. S. Sumerlin, W. G. Sawyer, T. E. Angelini, *Sci. Adv.* **2017**, *3*, e1602800; e) R. L. Truby, J. A. Lewis, *Nature* **2016**, *540*, 371; f) A. Lee, A. R. Hudson, D. J. Shiwardski, J. W. Tashman, T. J. Hinton, S. Yerneni, J. M. Bliley, P. G. Campbell, A. W. Feinberg, *Science* **2019**, *365*, 482.
- [17] S. Abdollahi, A. Davis, J. H. Miller, A. W. Feinberg, *PLoS One* **2018**, *13*, e0194890.
- [18] a) I. El-Katraty, S. H. Masood, Y. S. Morsi, *Rapid Prototyping J.* **2010**, *16*, 36; b) D. Ibrahim, T. L. Broilo, C. Heitz, M. G. de Oliveira, H. W. de Oliveira, S. M. W. Nobre, J. H. G. dos Santos Filho, D. N. Silva, *J. Cranio-Maxillofac. Surg.* **2009**, *37*, 167; c) M. Salmi, K.-S. Paloheimo, J. Tuomi, J. Wolff, A. Mäkitie, *J. Cranio-Maxillofac. Surg.* **2013**, *41*, 603; d) D. N. Silva, M. Gerhardt de Oliveira, E. Meurer, M. I. Meurer, J. V. Lopes da Silva, A. Santa-Bárbara, *J. Cranio-Maxillofac. Surg.* **2008**, *36*, 443; e) A. Unkovskiy, S. Spintzyk, D. Axmann, E.-M. Engel, H. Weber, F. Huettig, *J. Prosthodontics* **2019**, *28*, e460.
- [19] R. Eftekhar Ashtiani, L. Nasiri Khanlar, M. Mahshid, A. Moshaverinia, *J. Prosthet. Dent.* **2018**, *119*, 233.
- [20] A. Unkovskiy, S. Spintzyk, D. Axmann, E. M. Engel, H. Weber, F. Huettig, *J. Prosthodontics* **2019**, *28*, e460.
- [21] B. Fahy, S. Lareau, M. Sockrider, in *Am J Respir Crit Care Med, American Thoracic Society*, **2011**, 1.
- [22] a) M. D. Bartlett, E. J. Markvicka, C. Majidi, *Adv. Funct. Mater.* **2016**, *26*, 8496; b) T. Lu, E. J. Markvicka, Y. Jin, C. Majidi, *ACS Appl. Mater. Interfaces* **2017**, *9*, 22055.
- [23] a) E. M. C. Hillman, *J. Biomed. Opt.* **2007**, *12*, 051402; b) J. Kainerstorfer, A. Sassaroli, S. Fantini, *J. Biomed. Opt.* **2016**, *21*, 101408; c) P. D. Mannheim, *Anesth. Analg.* **2007**, *105*, S10.
- [24] S. Prahl, Optical Absorption of Hemoglobin, omlc.org/spectra/hemoglobin (accessed: June 2018).
- [25] M. Kohl, C. Nolte, H. R. Heekeren, S. Horst, U. Scholz, O. Hellmuth, V. Arno, *Phys. Med. Biol.* **1998**, *46*, 1771.

## Supporting Information

## 3D Printing Silicone Elastomer for Patient-Specific Wearable Pulse Oximeter

Sara Abdollahi, Eric J. Markvicka, Carmel Majidi, Adam W. Feinberg\*

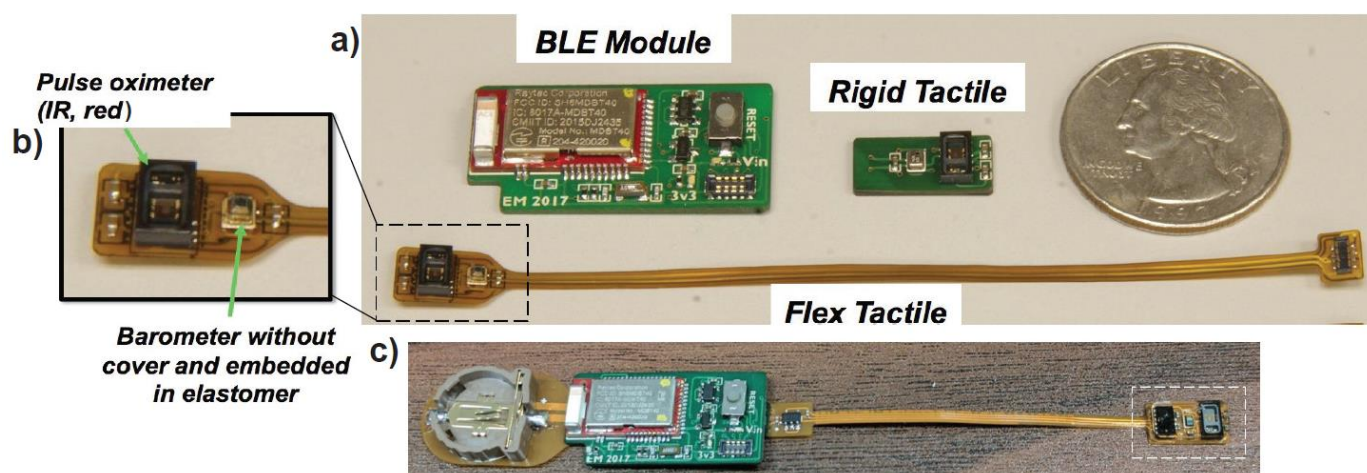


**Figure S1. Pulse oximetry & pressure sensing fPCB for the P<sup>3</sup>-wearable.** (a) Representative image of the flex tactile fPCB in comparison with a rigid tactile shown separately. The Bluetooth low energy (BLE) module is also shown. (b) Close-up of the fPCB, specifically of the section incorporated in the window cutout of the 3D printed flexible patient-specific cuff. The fPCB components include the pulse oximeter chip (*MAX30102*, Maxim Integrated) with LEDs (IR, red), and a barometric chip for pressure sensing. (c) Schematic of the assembled device including an insert for the coin cell battery that powers it.

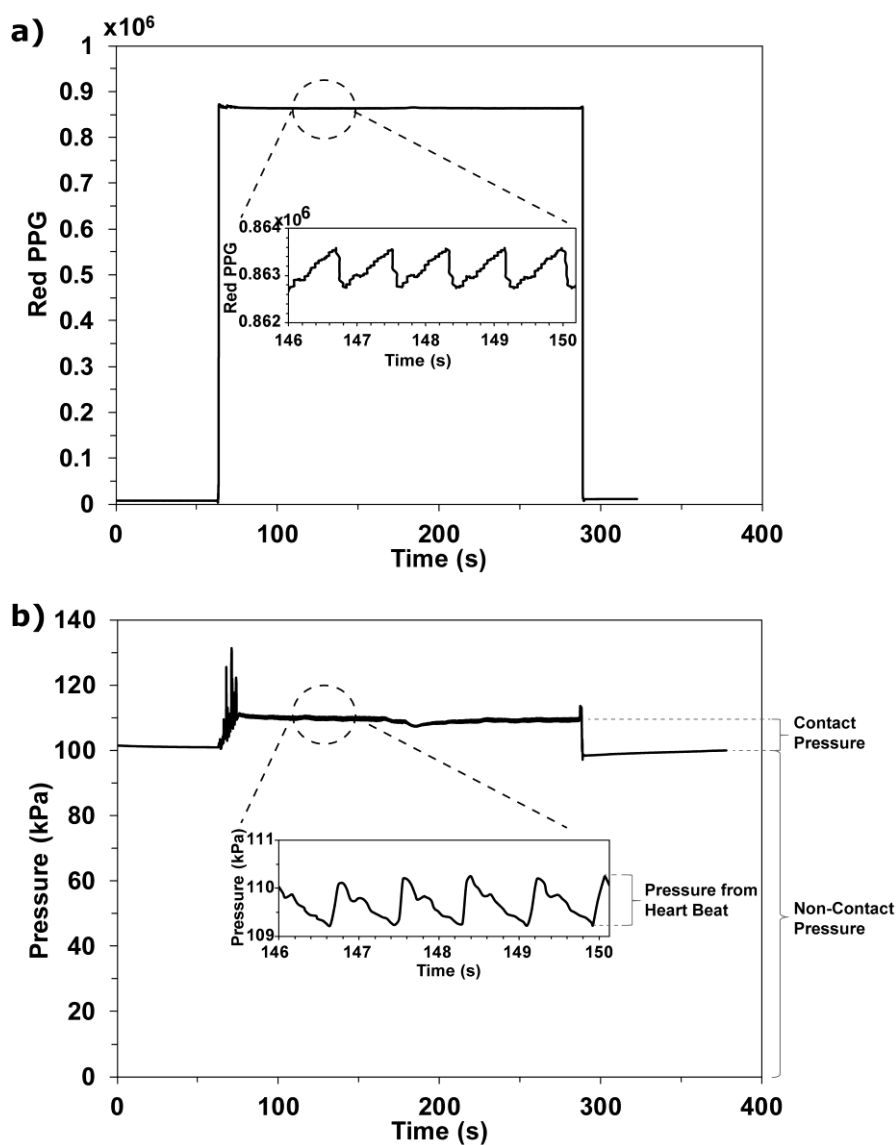


**Figure S2. Raw recordings from the wearable pulse oximeter displaying the three stages detached-worn-detached for (a) the photoplethysmographic (PPG) signals from the red LED, and (b) the pressure signals from the barometer. Recordings could be viewed simultaneously on the tablet and were measured using the cuff size 100% to the dimensions of the finger.**

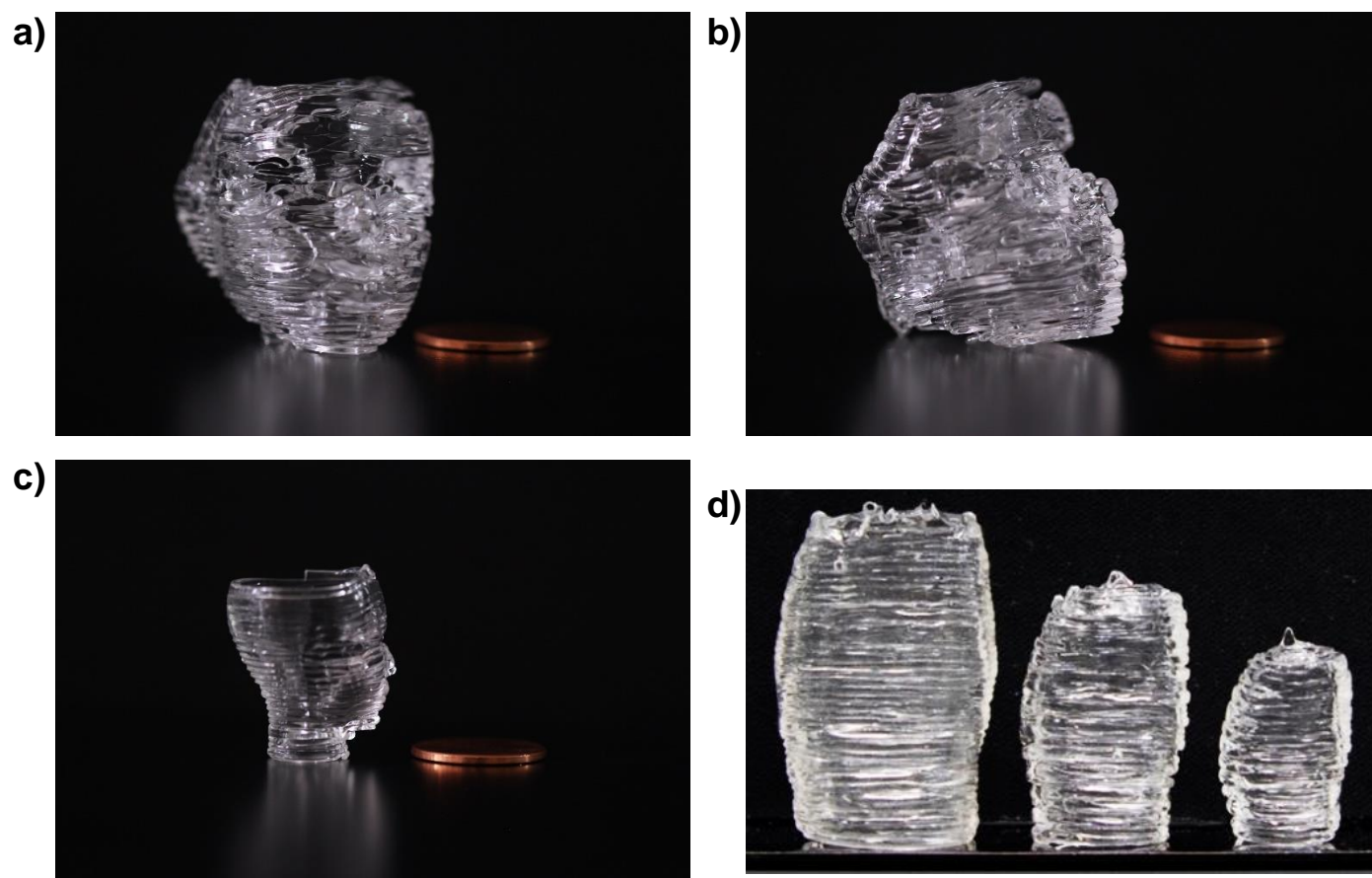


**Figure S3. Examples of additional complex shapes 3D printed from silicone (Sylgard 184) using the FRE technique.** Photographs show small prints 1-2 inches high of (a) a face front view, (b) a face side view, (c) a head profile, and (d) a large toe 3D printed at full size (left) and then scaled-down to two smaller sizes (middle, right). A U.S. penny is used for an indication of scale.

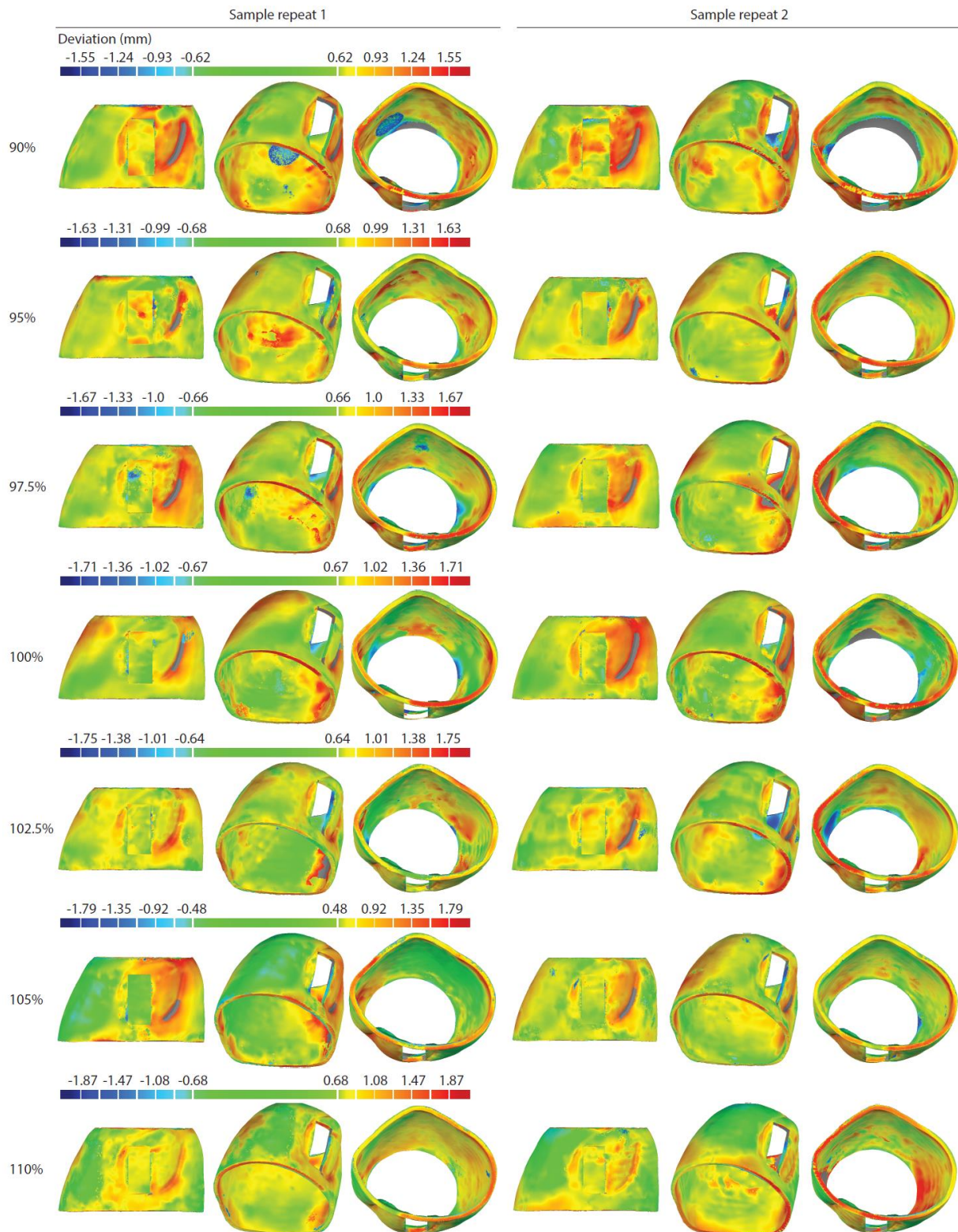


**Figure S4. Dimensional accuracy of the toe cuff sizes.** Heat maps showing the deviation of the original and reverse-engineered CAD models across the 90%, 95%, 97.5%, 100%, 102.5%, 105%, and 110% cuff sizes ( $n = 2$ ).

**Table S1. Dimensional accuracy of the 100% size printed toe cuff.** Deviation and surface area analysis of the digitized print and original CAD models. For the first print repeat, Toe 1, the average CAD-Print deviation was 0.67 mm and that of the second print repeat, Toe 2, was 0.65 mm. A larger sample size provides for a more robust deviation analysis. Still, these two measurements are in good agreement despite the potential errors from the imaging modality and those that stem from the reverse engineering process. These errors may also lead to artifacts that contributed to the 2.9% to 4.4% differences between the CAD-Print surface areas.

Cuff size	Print repeats	Maximum positive deviation (mm)	Maximum negative deviation (mm)	Mean positive deviation (mm)	Mean negative deviation (mm)	Average deviation (mm)	Surface area (mm <sup>2</sup> )	Surface area difference <sup>1</sup> (%)
100%	Toe 1	1.72	-1.72	0.77	-0.55	0.67	4023	2.9
	Toe 2	1.71	-1.71	0.79	-0.50	0.65	4082	4.4

<sup>1</sup>Original CAD surface area = 3910 mm<sup>2</sup>; Surface area difference (%) = [(print CAD – original CAD)/original CAD] × 100